## A NMF-based non-Euclidean Adaptive Feature Extraction Scheme for Limb Motion Pattern Decoding in Pattern Recognition System

Frank Kulwa; Pengrui Tai; Doreen S Sarwatt; Mojisola G Asogbon; Rami Khushaba; Tolulope T Oyemakinde; Sunday T Aboyeji; Guanglin Li\*; Oluwarotimi W Samuel\*; and Yongcheng Li\*

Abstract— Feature extraction is a crucial step in electromyogram (EMG)-based pattern recognition systems for decoding motor intents. However, despite the existence of numerous proposed techniques for feature extraction, their decoding performances have remained relatively low. Furthermore, these techniques are often evaluated without taking into account the drift between the training and test datasets. This study proposes a feature extraction scheme that operates in an unsupervised manner to address these limitations. This approach focuses on reducing drift between the training and test sets by utilizing feature adaptation based on non-negative matrix factorization (NMF) and Riemann operations. Additionally, we minimize drift by aligning the distribution of the test data with that of the training set. The results demonstrate that the proposed feature extraction technique exhibits significantly higher performance (p < 0.05) in decoding motor intent for 13 hand and finger movements, achieving an average accuracy of 99.91 ± 0.35% for amputee participants and 99.99  $\pm$  0.02% for able-bodied participants. We also conducted further investigations to assess the effectiveness of the proposed feature scheme against varied signal-to-noise ratios (SNRs). These investigations revealed that our technique outperforms other feature extraction techniques in terms of decoding performance, even in the presence of varied SNRs. Overall, the findings show that the proposed feature extraction technique can effectively enhance the reliability and robustness of EMG control systems in both clinical and commercial applications.

*Index Terms*— Symmetric positive definite (SPD) matrices, Electromyogram (EMG)-based prosthesis, Pattern recognition, Nonnegative matrix factorization (NMF), Non-Euclidean manifold.

## I. INTRODUCTION

In recent times, there has been increasing research attention towards the application of electromyogram (EMG)-based pattern recognition (PR) techniques, specifically for facilitating control in prostheses, gaming, and rehabilitation systems [1], [2]. PR-based pipelines consist of interconnected

phases that collectively aid in the adequate recognition of distinct muscle activation patterns associated with various EMG signal signatures of limb movement. Studies have shown that each phase of the pipeline influences the decoding outcome of movement signatures and the stability of the PR control scheme. Moreover, it has been demonstrated in previous studies that the feature vector construction phase has a greater impact than the other phases of the PR-driven scheme [3]. Additionally, effective PR-based control schemes ideally assume that the myoelectric signal patterns of specific limb movements exhibit both distinctiveness and reproducibility across multiple trials. These signal patterns are also expected to differ from the patterns observed in other movements [4], [5]. Therefore, the construction of a feature vector needs to take into consideration accurate and robust descriptors that can capture possible motor information from the EMG signals for robust movement characterization. Notably, such a feature vector would not only aid in the proper characterization of movement intention in research settings but also in the practical deployment of PR-based control schemes in miniaturized assistive or rehabilitation robots.

In the pursuit of a robust PR-based control scheme, existing studies have employed diverse feature extraction techniques. For instance, He et al. introduced a frequency-dependent feature set that was applied to characterize the myoelectric signals of various patterns [6], while Khushaba et al. proposed a time-dependent spectral moment-driven feature set for forearm and hand gesture decoding [7]. Similarly, Hudgins et al. proposed four classical time-domain descriptors, which are considered benchmark features for EMG-based movement signature classification [8]. Likewise, Samuel et al. introduced a spatial-temporal feature set, which was used to characterize

This work was supported in part by the Ministry of Science and Technology of China under grants (STI2030-Brain Science and Brain-Inspired Intelligence Technology-2022ZD0210400), GUANGDONG TALENTS PROGRAM (2023QN10Y209), Guangdong Provincial Key Laboratory of Multimodality Non-Invasive Brain-Computer Interfaces (Grant no. 2024B1212010010), Shenzhen Strategic Emerging Industry Support Plans (XMHT20230115002), Guangdong Basic and Applied Basic Research Foundation (\#2023A1515011478), and Major Basic Research Project of Shandong Natural Science Foundation (ZR2021ZD40), CAS President's International Fellowship Initiative (2024PVB0025). For the purpose of Open Access, the author has applied a Creative Commons Attribution (CC BY) public copyright license to any Author Accepted Manuscript version arising from this submission.

- F. Kulwa is with the Department of Rehabilitation Medicine, Shenzhen Hospital, Southern Medical University, Shenzhen, China, 518101
- T. T Oyemakinde, S.T. Aboyeji, F. Kulwa, G. Li, O.W. Samuel, and Y.C. Li are with the CAS Key Laboratory of Human-Machine Intelligence-Synergy Systems and the Shenzhen Institute of Artificial Intelligence and Robotics for Society, Shenzhen Institute of Advanced Technology (SIAT), Chinese Academy of Sciences (CAS), Shenzhen,

Guangdong 518055, China. (Correspondence: Dr. Li Yongchen, e-mail: <a href="mailto:li.yc@siat.ac.cn">li.yc@siat.ac.cn</a>, Dr. Oluwarotimi Williams Samuel, e-mail: <a href="mailto:o.samuel@derby.ac.uk">o.samuel@derby.ac.uk</a> and Dr. Guanglin Li, e-mail: <a href="mailto:gl.li@siat.ac.cn">gl.li@siat.ac.cn</a>.

- G. Li and Y.C. Li are also with the Guangdong Provincial Key Laboratory of Multimodality Non-Invasive Brain-Computer Interfaces.
- T. T Oyemakinde, and S.T. Aboyeji are also with the Shenzhen Institute of Advanced Technology, University of Chinese Academy of Sciences, Shenzhen, Guangdong 518055, China.
- O.W. Samuel and M.G. Asogbon, are with School of Computing, University of Derby, Derby, DE22 3AW, UK. O.W. Samuel is also with INTI International University, Nilai,71800. Malaysia.

Pengrui Tai is with Brain Cognition and Brain-Computer Intelligence Integration Group, Kunming University of Science and Technology, Kunming 650500, China D. S. Sarwatt is with University of Science and Technology Beijing, China. R. Khushaba is with Transport for NSW, Alexandria, Nsw, Australia

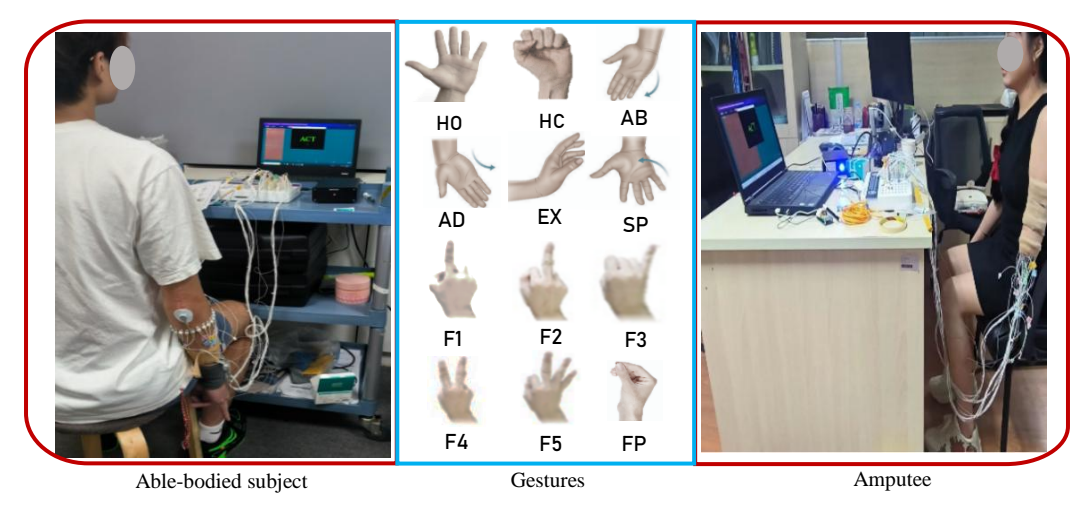


Fig 1. Electrode configuration and the gestures involved in data collection.

the movement intentions of amputees and able-bodied subjects from EMG recordings [9].

Despite the contributions of these methods and many others towards enhancing the control of PR-driven prostheses, gaming, and rehabilitation systems, their practical adoption in commercial and clinical settings is limited. This limitation is partly due to the fact that existing feature vector construction approaches are rarely high-performing. This can be attributed to the discrepancy (drift) between the training and testing sets, which might be caused by factors such as the non-stationary nature of the EMG signals and variation in signal-to-noise ratios (SNR) induced by external factors during the testing phase [39], [10]. Specifically, in the benchmark EMG data acquisition protocol, prior to the data collection task, the subjects' limbs are cleansed with alcohol pads, particularly the area overlaying the arm muscle where the signal sensors are placed [20, 40, and 41]. The EMG signals are then collected and used for training and testing the classifier. However, in real or clinical applications of prosthesis or rehabilitation device, only the data used for training the classifier can be prepared in such a well-controlled environment. In contrast, during the classifier's testing phase, issues such as the presence of hair between the electrode and skin, dust accumulation, and drying of the electrolyte/gel arise [42, 43, 44]. These factors increase the impedance or electrical resistance between the skin and electrode contact, which also contributes to the discrepancy between the training and testing data, further degrading the overall performance of the classifier.

Table 1. The detailed information of the amputees subjects

Amputee	Gender	Age	Length of residual arm from the elbow
1	Female	26	14.5cm
2	Female	27	5.3cm
3	Female	30	7.4cm
4	Female	31	6.0cm
5	Male	28	4.6cm
6	Male	40	10.4cm
7	Male	35	12.3cm
8	Male	37	9.7cm
9	Male	42	7.7cm
10	Male	47	8.6cm
11	Male	29	13.0cm
12	Male	27	11.3cm
13	Male	25	11.6cm
14	Male	38	6.6cm
15	Male	38	5.1cm

Therefore, in this research, a novel unsupervised descriptor extraction scheme is designed to effectively decode motor information in both clean datasets and in the presence of varied SNR. Specifically, the proposed scheme first leverages nonnegative matrix factorization (NMF) due to its ability to represent muscle synergy (activation potential) from EMG signals while reducing non-stationarity [15][17]. It has been shown that high-dimensional data (such as EEG and EMG) exist in a non-Euclidean space. Applying Euclidean operations to such data may overlook important information. However, using non-Euclidean operations, such as those in Riemannian geometry, is more suitable, as they can uncover the underlying structure of complex data [50], [51]. Although these manifolds have been extensively applied in other domains, such as EEG [50] and image processing [52], they have rarely been used in mining EMG data, especially for upper limb movement decoding. Therefore, the second stage of the proposed scheme incorporates symmetric positive definite matrices (SPD) as descriptors, since SPD matrices exist in Riemannian space. To reduce the drift between the testing and training datasets, all the SPDs (from the testing and training datasets) are projected towards a Riemann mean (which is derived from the training set only). In the third stage, the approach reinforces robust adaptation by projecting the features from the previous stage toward a shared distribution derived from the training dataset. The combination of these operations contributes to the improvement of movement decoding performance.

The performance of the proposed scheme was validated using a novel dataset which was collected from both amputee and able-bodied subjects as described in the section II-A.

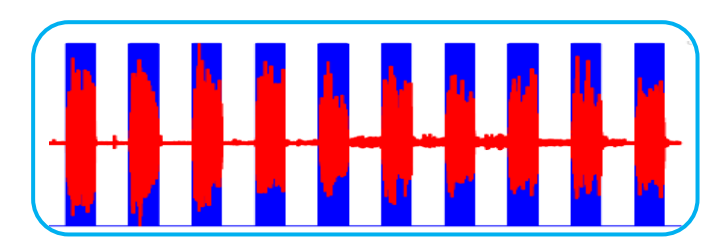


Fig. 2. EMG signal (in red) and a synchronization signal (in blue)

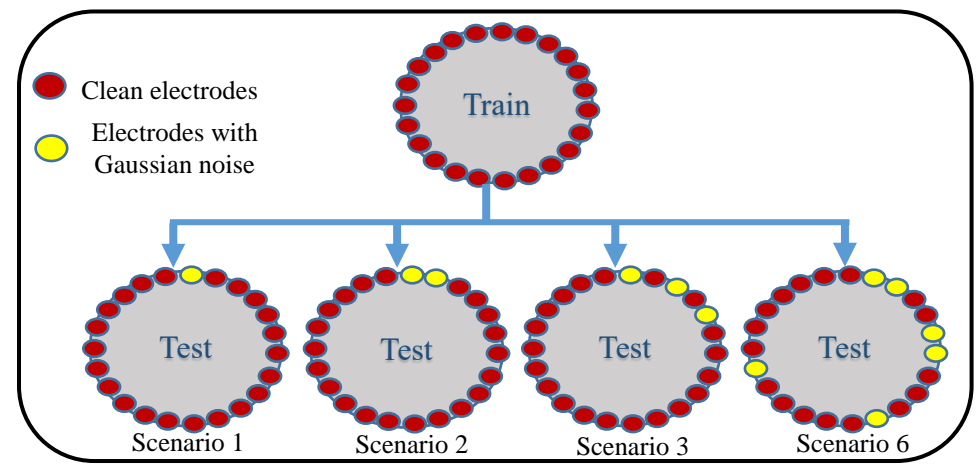


Fig 3. Configuration of clean electrodes and electrodes with noise at different experimental scenarios.

#### II. MATERIAL AND METHODS

#### A. Data Collection

The electromyogram recordings were collected from a total of 35 individuals, including 20 able-bodied participants and 15 transradial amputees (ages:  $30.0 \pm 10.5$  years) who participated in the experiment. Table 1 summarizes information about the amputees. Prior to the start of the experiment, the participants signed consent agreement forms, and the research protocol was reviewed and approved by the Institutional Review Board at the Shenzhen Institute of Advanced Technology, Chinese Academy of Sciences, with IRB number SIAT-IRB-221115-H0626.

The dataset was collected using an EMG acquisition device (NES-128B01, 64 channels, and a sample rate of 2 kHz, designed by the Research Center for Neural Engineering, SIAT, CAS, China). A total of 24 individual electrodes were placed around the dominant forearm, just below the elbow, with an approximate spacing of 10 millimeters between each electrode, as illustrated in Figure 1. Throughout the data collection process, a computer was positioned infront of the participants to instruct the participants to perform specific wrist and finger gestures, totaling 13 movement tasks (Fig. 1). These gestures were selected due to their significance in upper-limb motor tasks [21]. The gestures included Hand Open (HO), Hand Close (HC), Abduction (AB), Adduction (AD), Extension (EX),

Supination (SP), Extending the index finger (F1), Extending the middle finger (F2), Extending the little/pinky finger (F3), Extending both the index and middle fingers (F4), Extending the last three fingers (F5), Fingers Pinch (FP), and No Motion (NM). Each gesture was performed 10 times, with each motion trial lasting approximately 6 seconds, followed by an 8-second rest period between consecutive trials. The data were collected at a sampling rate of 2000 hertz. Additionally, a 50 hertz notch filter was applied, along with a bandpass filter that had cutoff frequencies of 10 to 500 hertz. This filtering process was employed to extract the relevant signal components from the data. In order to help synchronize the onset phase and rest/idle periods for each trial during signal acquisition, a separate signal was incorporated to indicate the start and end of the onset phase and rest phase, as conceptualized in Fig. 2. This would aid in chopping/segmenting the onset (active) part of the signal during signal processing.

### B. Electrode Configurations

During data analysis, 9 trials (out of 10 trials) were used for training, while 1 trial was used for testing. Similar experiments were repeated 5 times, with different trials considered for testing each time (i.e., trials 1, 3, 5, 7, and 9), and the results were recorded as averages for all five trials.

To depict real practical/clinical scenarios where the training of the decoding system occurs in a controlled environment, while the practical application (testing) of the system is Table 2. Specific electrodes to which noise was added in different scenarios for both amputees and able-bodied subjects

	1 <sup>st</sup> time	2 <sup>nd</sup> time	3 <sup>rd</sup> time	4 <sup>th</sup> time	5 <sup>th</sup> time
Scenario 1	5	2	16	11	23
Scenario 2	8 and 17	5 and 22	12 and 19	3 and 21	9 and 14
Scenario 3	3,7, and 16	1,12, and 20	9, 11, and 18	5, 14, and 23	2,15, and 19
Scenario 4	4, 10, 17, and 21	5,9,14, and 23	3, 7, 12, and 19	2, 8, 16, and 22	1, 6, 13, and 18
Scenario 5	5,8, 13, 18, and 24	3,7,9,14, and 21	2,6,10,15, and 20	4,11,12,19, and 23	1,6,16,17, and 22
Scenario 6	2,4,7,14,19, and 22	3,5,9,11,17, and 20	1,6,12,13,18, and 23	8,10,15,16,21, and 24	4,6,10,14,19, and 23
Scenario 7	3,5,9,12,17,19, and 21	2,4,6,10,15,20, and 23	1,7,8,11,14,18, and 22	3,5,13,9,16,21, and 24	2,4,6,10,12,17, and 19
Scenario 8	4,7,8,12,14,16,19, and 23	3,5,6,9,11,18,21, and 24	1,2,10,13,15,17,20,and 22	3,5,7,8,12,16,19, and 24	1,2,9,13,15,18,20, and 22
Scenario 9	1,4,7,8,10,14,17,21, and 23	3,5,6,9,11,12,15,19, and 24	1,2,7,9,13,16,18,20, and 22	2,5,8,10,11,13,15,19, and 23	3,4,6,12,14,16,17,21, and 24
Scenario 10	2,4,7,9,11,12,16,18,20, and 22	3,5,6,10,13,14,17,19,21, and 23	1,3,6,8,10,13,15,17,22, and 24	2,4,7,9,11,12,16,18,20, and 22	3,5,6,10,13,14,17,19,21, and 23
Scenario 11	3,4,5,7,9,10,12,16,18,20, and 22	1,3,6,8,11,13,14,17,19,21, and 23	1,6,7,9,12,13,15,16,20,22, and 23	2,3,5,8,10,11,14,18,19,21, and 24	4,5,7,8,10,12,13,16,17,20, and 22
Scenario 12	2,4,6,7,9,11,12,14,16,18,2 0, and 22	1,3,5,6,8,10,13,14,17,19,2 1, and 23	1,3,6,8,10,12,13,15,17,19, 22, and 24	2,4,5,7,9,11,12,14,16,18,2 0, and 22	3,5,6,8,10,13,14,15,17,19, 21, and 23

subjected to uneven signal drifts due to changes or increases in impedance between the electrode and the skin. White Gaussian noise (WGN) was added to different electrodes of the test set only, following a predefined random sequence indicated in Table 2. Meanwhile, all electrodes in the training set were kept clean and free of noise, as indicated in Fig. 3.

Twelve scenarios were considered: in scenario 1, only one electrode was subjected to noise, and the experiment was repeated 5 times with a different electrode selected each time. Scenario 2 involved two electrodes at a time, and similarly, the experiment was repeated 5 times while considering different electrodes each time. Scenario 3 involved 3 electrodes, with a protocol similar to scenarios 1 and 2. Scenario 4 involved four electrodes, and scenario 5 involved five electrodes. The scenarios continued up to scenario 12, where twelve random electrodes were subjected to noise. Table 2 indicates the different scenarios.

### C. Feature extraction

In this study, a novel robust descriptor extraction technique was proposed for the effective characterization of EMG signals, even in the presence of uneven variations in signal-to-noise ratios. We denote this scheme/features as the NMF-based Non-Euclidean Riemannian Descriptor (NNERD). The key steps for the extraction of the NNERD are described in the following subsections. Fig. 4 summarizes the major steps of the proposed feature extraction technique.

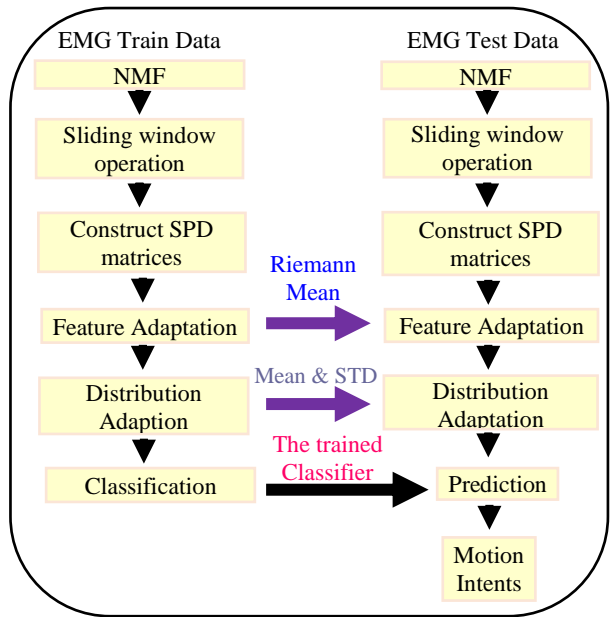


Fig 4. The Flow chart for the proposed technique

#### (i) Non-negative Matrix factorization (NMF)

NMF, or Non-negative Matrix Factorization, is an effective algorithm for multivariate data analysis. It can decompose any matrix with non-negative values into two separate matrices, both of which contain only non-negative elements. Inspired by its ability to reduce the non-stationary nature of the signal [17], we first apply it to the raw signal before segmenting it. The operation of NMF can be expressed as follows:

Consider a matrix Z (which represents the EMG signal) given by:

$$Z \in \mathbf{R}^{n \times m}$$
; if  $\mathbf{R} > 0$  (1)

Here, for the training set, R consists of all non-negative elements of all nine trials of a specific movement, while for the test set, R represents non-negative elements of one trial of a specific movement, n is the number of features, while m is the size of samples. Precisely, in this study n=24 (equivalent to the number of electrodes) and m is the size of discrete data points. It is worth noting that, before the NMF operation, all the negative values of the EMG signal (R) were suppressed to be equal to zero. The NMF can linearly decompose a matrix Z into two matrices. A basic matrix  $W \in R^{n \times k}$  and a coefficient matrix  $H \in R^{k \times m}$ . Specifically, the (m, n)-th element of Z,  $z_{nm}$ , is calculated as;

$$Z_{nm} \approx (W \cdot H)_{nm} = \sum_{k=1}^{k} W_{nk} H_{km}$$
 (2)

Choosing the value of k is very necessary for balancing both complexity and performance. Thus, in this study, we used k = 12 as it showed higher performance than others.

It should be noted that after the NMF operation, the signals were segmented into overlapping chunks following the sliding window operation [16]. Specifically, they were segmented into overlapping windows of size 150 ms, with an overlap of 50 ms. Thus, let each signal chunk (segment) be represented as;  $X \in X^{n \times q}$  here n represents the number of channels in the data, and q the number of samples in one segment/chunk.

## (ii) Construction of the Sample Covariance Matrices (SCM)

Given the EMG signal  $X \in X^{n \times q}$ , we can estimate the sample covariance matrix (SCM) represented as  $S \in R^{n \times n}$  by deploying Equation 3. To estimate the SCM, we utilized a regularized estimator known as oracle approximating Shrinkage (OAS) as it showed comparatively higher performance than other estimators such as Ledoit Wolf, and Schaefer Strimmer [11], [12].

$$S = \frac{XX^T}{trace(XX^T)} \tag{3}$$

As concluded by Yger et al. [13], the SCM belongs to the symmetric positive definite (SPD) space, indicating that its eigenvalues are strictly positive. Thus, we used the constructed SCM as SPD and denoted it as S(n) with size  $n \times n$  (24 × 24).

Riemannian Manifold (RM): According to the literature [26], the RM is defined as a smooth manifold where the tangent space at any point is the Euclidean space of infinite dimension. The classification of symmetric positive definite matrices (SPD) as RM has facilitated the use of Riemannian operations on SCM [14], [23]. The novel descriptor adaptation technique proposed is built upon the following key definitions.

Geodesic path  $(\delta_{\gamma})$ : It is the shortest path between two SPD matrices (such as  $S_1$  and  $S_r$ ) on the RM. It describes how one can traverse (project) from  $S_1$  towards  $S_r$  and vice versa [24]. According to Moakher et al. [25], the geodesic path

between two matrices (SPDs) can be estimated using Equation 5.

$$\gamma(S_1, S_r, t) = S_1^{\frac{1}{2}} \left( S_1^{-\frac{1}{2}} S_r S_1^{-\frac{1}{2}} \right)^t S_1^{\frac{1}{2}} \quad t \in (0, 1)$$
 (4)

Here, t is a hyper-parameter which defines the direction of traverse, either more towards  $S_1$  or  $S_r$ , and it needs to be tuned. It is worth noting that in our preliminary analysis, we found t = 0.5 exhibits high and consistent decoding performance compared to other possible t values.

**Tangent space** (S): Is the space demarcated by the whole set of tangent vectors  $P_i$ . In this manifold, the metric embodies a Euclidean flat structure that allows the application of conventional mathematical (arithmetic) operations such as mean, variance, etc.

Assuming  $S \in S(n)$  being a point that belongs to the manifold of the SPDs (which is embedded in a RM), it is feasible for each point  $S_i \in S(n)$  to associate a vector (a tangential vector)  $P_i \in P(n)$  which belongs to the tangent space, such that  $P_i = \gamma(0)$ . Here,  $\gamma(t)$  is a geodesic between S and  $S_i$ . The Riemann logarithmic (Log) map operator denoted as  $Log_s: S(n) \to P(n)$  facilitates the mapping of point  $S_i$  to its corresponding tangent vector  $P_i$  conversely the Riemannian exponential (Exp) map operator  $Exp_s: (P_n) = S_n$  allows a bijective mapping from the tangent manifold (space) to the original space of SPDs S(n). Utilizing the AIRM [22], the Riemannian logarithm (Log) and exponential (Exp) map operations can be expressed as;

$$Exp_{S}(P_{i}) = S^{\frac{1}{2}}Exp(S^{-\frac{1}{2}}P_{i}S^{-\frac{1}{2}})S^{\frac{1}{2}}$$
(5)

$$Log_{S}(S_{i}) = S^{\frac{1}{2}}Log(S^{-\frac{1}{2}}S_{i}S^{-\frac{1}{2}})S^{\frac{1}{2}}$$
(6)

**NB:** The projection of symmetric positive definite matrices from the RM to the corresponding tangent space, and the reverse operation from the tangent space back to the manifold, can be achieved using the expressions given in Equations 5 and 6, respectively.

## (iii) Feature Adaptation (FA)

In reducing/removing the discrepancy between the training and testing set, all high-dimensional signals were subjected to the NMF operation, and then every segment (of size  $24 \times 150$ ) in both training and testing dataset was converted to SPD (belonging to RM space) using Equation 3. Then, using the reference point  $S_r$  (in this study, we used a Riemann mean of the training set only as a reference), every SPD was projected towards a Riemann mean ( $S_r$ ) as expressed in Equation 4. The output of this stage is represented as  $S_{train}$  and  $S_{test}$  for training and testing datasets, respectively.

Therefore, the Riemann mean  $(S_r)$  is estimated using equations 5 and 6 as outlined in Algorithm 1.

**Algorithm 1** Riemann Mean of m SPD matrices  $(S_r)$ 

Input: m SPDs 
$$\{S_1, S_2, S_3 \dots S_m\}$$
 and tolerance  $> 0$ 
Output: The estimated Riemann mean  $(S_r)$ 
Initialize:  $S_r^{(t)} = \frac{1}{m} \sum_{i=1}^m (S_i), t = 1$ 
While
$$\bar{S} = \frac{1}{m} \sum_{i=1}^m Log_{S_r^{(t)}}(\bar{S}_i)$$

$$S_r^{(t+1)} = Exp_{S_r^{(t)}}(\bar{S})$$

$$t = t+1$$
Until  $\|S_r^{(t+1)}\|F < \in$ 
Return  $S_r^{(t+1)}$ 

It should be noted that only the SPDs from the training set were used to find the Riemann Mean  $(S_r)$ . The reason for using the Riemann mean instead of the arithmetic mean is that the Riemann mean of SPD matrices is guaranteed to be SPD, whereas the arithmetic mean of SPD matrices may not necessarily yield an SPD matrix.

#### (iv) Distribution adaptation (DA)

To further reduce the drift between the testing and training datasets, in this final step we projected all descriptors to the common distribution (specifically to the training set's distribution) by using the common standard deviation D and mean U derived from the training set only, as expressed in Equation 7. The input to this stage consists of the outputs from the previous stage,  $S_{test}$  for the testing set and  $S_{train}$  for the training set.

$$Z_{test} = \frac{S_{test} - U}{D}$$
 and  $Z_{train} = \frac{S_{train} - U}{D}$  (7)

where, 
$$U = \frac{1}{v} \sum_{i=1}^{v} (S_{train})$$
 (8)

and

$$D = \sqrt{\frac{(\sum_{i=1}^{v} (S_{train} - U))^2}{v}}$$
 (9)

From equations 7, 8, and 9,  $S_{train}$  represents the feature matrices of the training dataset, while v is the number of all features in  $S_{train}$ . Therefore, in the subsequent sections, we will be referring  $Z_{train}$  and  $Z_{test}$  as the *NMF-based Non-Euclidean Riemannian Descriptor (NNERD)*.  $Z_{train}$  and  $Z_{test}$  contain feature matrices of size  $n \times n$  (24 × 24). Before applying these features to the classification network (such as SVM), we flattened them to get each feature of size  $1 \times 576$ .

It is worth noting that the proposed scheme works in an unsupervised manner, as the optimization parameters (i.e., arithmetic mean, standard deviation, and Riemann mean) are derived from the training set only without any prior knowledge of the test set. Fig. 4 summarizes all operations.

#### D. Comparison to other State-of-the-art techniques

In order to compare the performance of the proposed feature, we considered a variety of multi-feature sets that have been used in previous research:

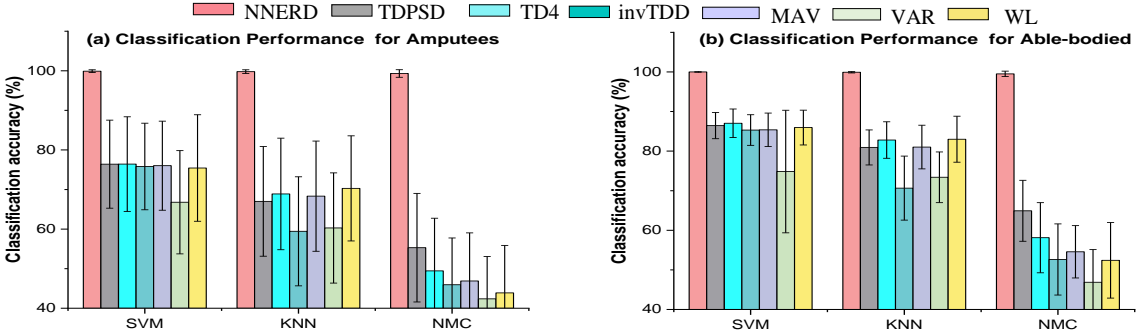


Fig 5. Classification accuracies of different features (NNERD, TDPSD, TD4, invTDD, MAV, VAR, and WL) applied on classifiers SVM, kNN and NMC when there is No Gaussian noise is added in both training and test set. (a) Indicates the decoding performance of amputees. (b)

Indicates the performance for the able-bodied subjects.

- 1. Invariant features in Time domain (invTDD): This approach combines five reliable time-dependent features that were introduced by Asogbon et al. to enhance decoding performance, even when there are variations in the muscle contraction forces [31].
- 2. Waveform Length (WL): This represents the total length of the signal waveforms within the given time window [29].
- 3. Time domain features (TD4): Is a set of commonly used time-dependent features which include wavelength, zero-crossings, slope sign change, and mean absolute value [4].
- 4. Time-Dependent Power Spectrum Descriptors (TDPSD): Is a descriptor composed of six features that estimate the power spectrum characteristics of the electromyogram signal directly from the time-domain [1].
- 5. Mean Absolute Value (MAV): This feature is estimated by taking the mean of the absolute values of the signal samples within the given time window [32].
- 6. Variance (VAR): is estimated by the variance of the EMG signal within the analyzed window. Specifically, it estimates the power of the electromyogram signal [33, 36]

The reason for using these techniques in comparison with the proposed approach is that they have been applied in previous works and have shown comparatively excellent decoding performance [17], [30], [34], [35]. To ensure a fair comparison, the same window size and stride were used during the extraction of the proposed technique and the comparative features (invTDD, WL, TDPSD, MAV, TD4, and VAR).

#### E. Basic Experimental Setups

To examine the decoding performance of the NNERD and compare it against other feature extraction techniques, three classifiers were used to decipher the inherent motion tasks: Support Vector Machine (SVM), Nearest Mean Classifier (NMC), and k-Nearest Neighbor (kNN) classifier [7, 27, 28]. kNN and SVM are commonly used in decoding EMG-based motor intents, while we have introduced the application of NMC for the first time in decoding motion intents in EMG signals due to its capability in handling high-dimensional features, the simplicity of the process, and the fact that it does not require parameter tuning [37, 38]. The analysis was conducted using two important metrics: accuracy and F1-score. We considered these metrics because they have been widely adopted in EMG-based motion classification works. Moreover, the F1-score encompasses recall and precision in its computation. The numerical definitions of these metrics are described in Equations 10 and 11.

$$Accuracy = \frac{TP+TN}{TP+FP+TN+FN}$$
 (10)

$$F1-score = \frac{2 \times Recall \times Precision}{Recall + Precision} = \frac{2TP}{2TP + FP + FN}$$
 (11)

Furthermore, a Friedman's test (non-parametric test) was performed, followed by a Dunn's post-hoc analysis, to assess the statistical significance of the proposed NNERD method.

### III. RESULTS ANALYSIS AND DISCUSSION

In this section, we describe a collection of investigations conducted to evaluate the efficacy of the NNERD and other-state-the-art descriptors.

Table 3: Classification F1-score of different features (NNERD, TDPSD, TD4, invTDD, MAV, VAR, and WL) applied on classifiers SVM, KNN, and NMC when there is no Gaussian noise added to both training and test set. The top results represent amputees' decoding performance while the bottom results represent the able-bodied decoding performance.

	Amputees								
	NNERD	TDPSD	TD4	invTDD	MAV	VAR	WL		
SVM	99.91±0.35	75.84±11.52	75.59±12.90	75.16±11.50	75.08±12.14	65.34±13.98	74.63±14.13		
KNN	99.79±0.47	66.20±14.18	68.11±14.61	58.64±14.04	67.04±14.76	58.64±14.39	69.71±13.56		
NMC	99.30±1.02	53.66±14.61	47.10±14.02	43.72±12.05	44.83±12.50	40.57±11.52	41.12±12.38		
Able-bodied subjects									
SVM	99.99±0.02	86.31±3.46	86.87±3.85	85.12±4.07	85.29±4.37	74.30±16.1	85.79±4.53		
KNN	99.91±0.18	80.63±4.61	82.56±4.75	70.16±8.13	80.21±6.04	72.26±7.07	82.56±6.23		
NMC	99.52±0.68	63.86±8.02	56.86±9.58	51.40±9.55	53.38±6.85	45.37±8.77	51.16±10.16		

A. Evaluation of the proposed method (NNERD) on decoding motion intents without considering the effects of varied SNRs

In this section, we analyze the decoding performance of the proposed feature scheme in the absence of noise in both the training and testing sets. We have considered this analysis because it is commonly employed in previous EMG-based decoding studies that do not consider the effects of noise [2, 31, 3]. It should be noted that during data analysis, 9 trials (out of 10 trials) were utilized for training, while one trial was used for testing. Similar experiments were repeated 5 times, with different trials being considered for testing at each time (i.e., trials 1, 3, 5, 7, and 9) and the results were recorded as the average of all five folds. The average classification accuracies for both amputee and able-bodied participants are shown in Fig. 5.

By closely examining the results in Fig. 5, we can observe that the NNERD has significantly (with p<0.05) performed better than all other features in both amputees (Fig. 5 (a)) and able-bodied subjects (Fig. 5 (b)). For instance, in Fig. 5 (a) on SVM classifier, the NNERD has outperformed other features, followed by TD4, TDPSD, MAV, invTDD, WL, and VAR with accuracies of 99.91±0.35%, 76.43±11.96%, 76.40±11.12%, 76.02±11.25%, 75.82±10.94%, 75.43±13.46%, 66.78±13.04%, respectively. Similarly, when considering the results for able-bodied subjects in Fig 5 (b) on the SVM classifier, the NNERD has attained an accuracy of 99.99±0.02%, while TD4, TDPSD, WL, MAV, invTDD, and VAR attained 87.05±3.60%, 86.45±3.32%, 85.95±4.39%, 85.38±4.22%, 85.32±3.87%, and 74.84±15.48%, respectively.

To conduct a more in-depth investigation of the features' performance, we analyzed the F1-score metrics, which are reported in Table 3. Based on the decoding results shown in Table 3, the NNERD approach demonstrated significantly (p < 0.05) superior performance compared to other features (TDPSD, TD4, invTDD, MAV, VAR, and WL) in both amputee and able-bodied subjects. These results (in F1-score) relate to the decoding results in accuracy and further justify the superiority of the proposed technique (*NNERD*).

## B. Evaluation of the proposed method (NERD) on decoding motion intents in the presence of varied SNR.

To depict the effects of uneven variation of SNR, which represents the effects of uneven changes of impedance between the electrode surface and the skin, Gaussian noise was added randomly to the electrodes as demonstrated in Section II-B. In this study, we considered three levels of noise (SNR) that have been recommended by Zhao et al. [39]. These levels are 0dB: which represents the highest level of noise when the signal level is equal to the noise level. 10dB: which represents a moderate level of noise, and 20dB, indicating the lowest noise. However, only the results for 0dB and 20dB were presented due to the consistent results displayed by 0dB and 10dB. The results for 0dB and 20dB are displayed in Fig. 6 and Fig. 7, respectively.

When looking into the results in Fig. 6 (0dB SNR) for both

amputees and able-bodied participants, it can be seen that the increase in the number of electrodes with noise affects the decoding performance of all features in all classifiers. Specifically for SVM and kNN classifiers, as the number of electrodes subjected to noise increases, the features NNERD, TDPSD, and TD4 show a decrease in accuracy while the invTDD, MAV, VAR, and WL portray unpredictable/inconsis-

tent performances. Although the proposed feature NNERD shows a small decrease in performance with the increase in electrodes with noise, its decoding performance is still very high compared to other features. For instance, the classification accuracies on SVM (Fig 6 (a)), when only one electrode is subjected to noise for amputees when different features are applied to SVM classifier are 99.87±0.39%, 75.14±10.91%,  $76.33\pm11.97\%$ ,  $76.03\pm10.98\%$ ,  $76.27\pm11.33\%$ ,  $67.43\pm13.54\%$ , and 75.45±13.72% for NNERD, TDPSD, TD4, invTDD, MAV, VAR, and WL, respectively. When twelve electrodes are subjected to noise (which is the worst-case scenario) the average accuracies are 93.36±6.27%, 65.91±11.51%, 75.10±9.51%, 75.53±10.83%, 77.45±10.28%, 69.07±13.57%, and 75.59±10.70% for NNERD, TDPSD, TD4, invTDD, MAV, VAR, and WL, respectively. A similar trend is observed in able-bodied configuration.

Regarding the NMC classifier, the performance trend is similar to that of SVM and kNN for the NNERD and TDPSD features, where the classification performance decreases (with a small margin for the proposed feature) with the increase in the number of electrodes with noise. However, features like TD4, invTDD, MAV, VAR, and WL show an opposite trend, starting with low accuracies and increasing with the number of electrodes with noise. Although their performances increase, they are still extremely low compared to the proposed NNERD. For instance, the performance (in accuracy) of the NNERD, TDPSD, TD4, invTDD, MAV, VAR, and WL features (for amputees Fig. 6 (c)) when one electrode is subjected to noise 98.92±1.06%, 55.13±13.46%, 50.14±13.39%. 46.19±11.86%, 47.40±12.13%, 42.78±10.58%, 44.38±12.13% accuracy, while the performance in the corresponding features when twelve electrodes are subjected to noise are, 92.32±5.43%, 49.24±12.21%, 54.65±13.66%, 51.29±12.21%, 49.29±11.98%, 46.65±10.59%, 49.48±12.60%, accuracy, respectively. The reason behind the higher decoding performances of NNERD compared to all other features might be due to the high dimensionality of the NNERD features, which works well for the NMC classifier.

It is worth noting that, although the varied SNR affects the features' decoding performance (at 0dB SNR), the proposed feature extraction scheme NNERD, has performed significantly (with p<0.05) better than other features in both amputees and able-bodied participants. This indicates the stability of the proposed feature to maintain higher performance even in the presence of noise.

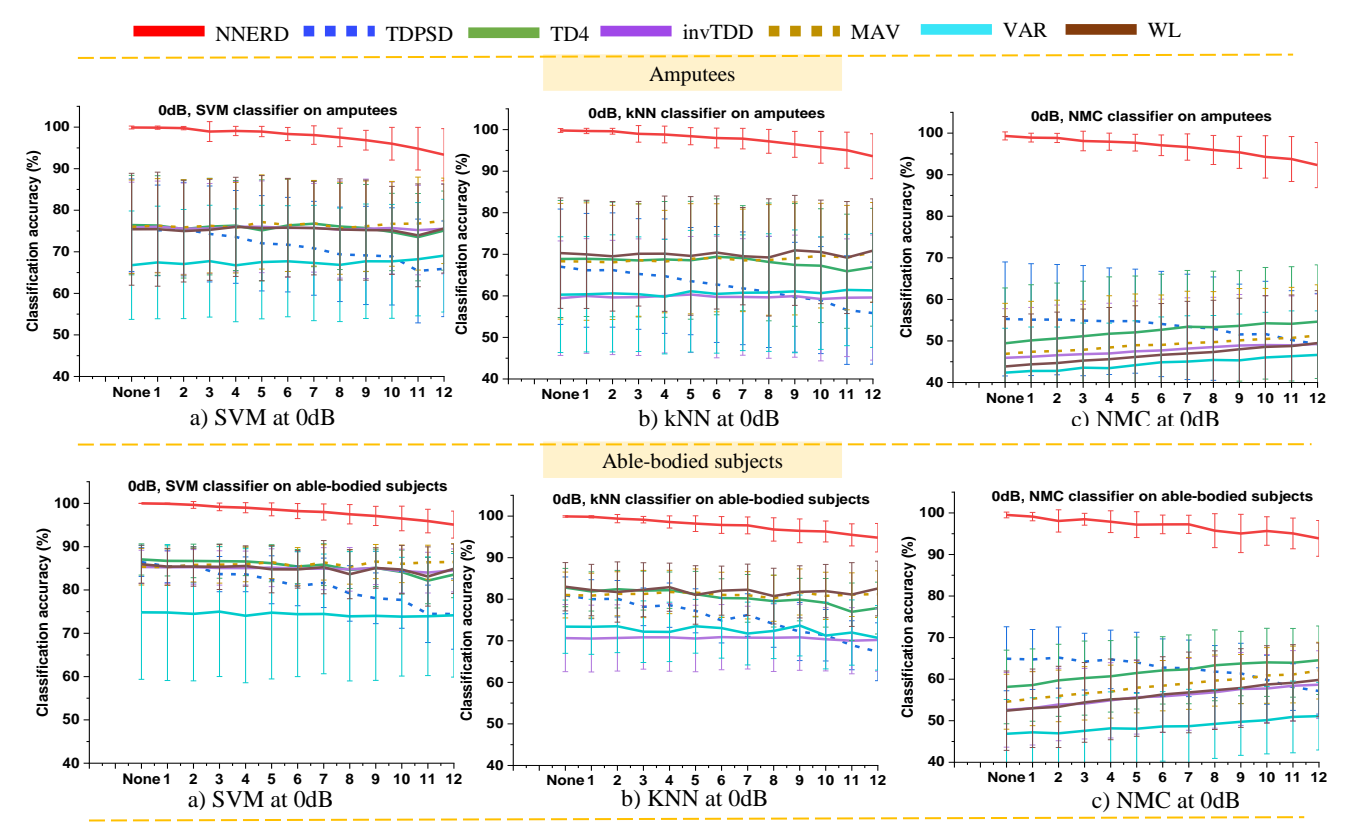


Fig 6. Classification accuracies of different features (NNERD, TDPSD, TD4, invTDD, MAV, VAR, and WL) applied on classifiers SVM, kNN and NMC when different number of electrodes of the test set are subjected to 0dB Gaussian noise. Note: The y-axis of all plots represent classification accuracies while the x-axis represent the quantity of electrodes with noise.

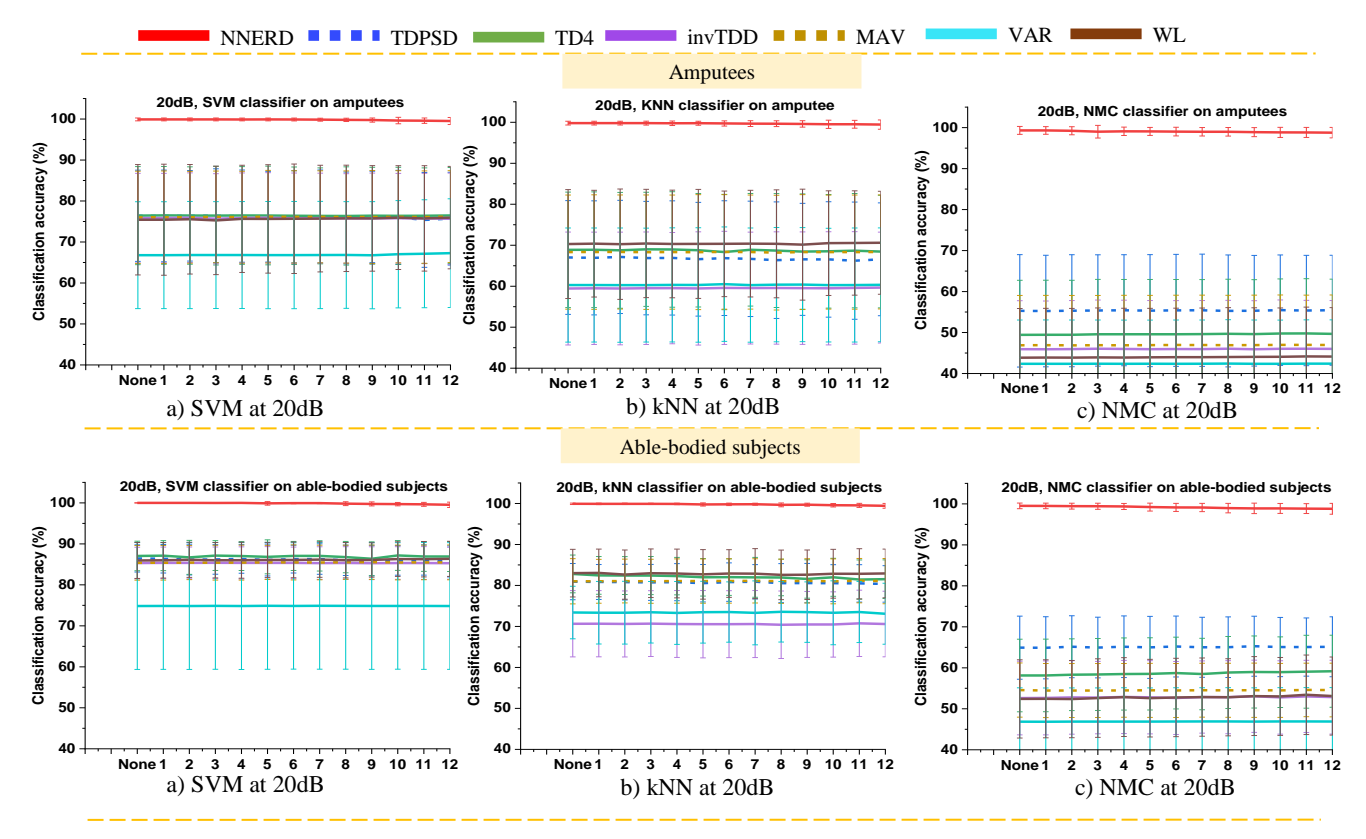
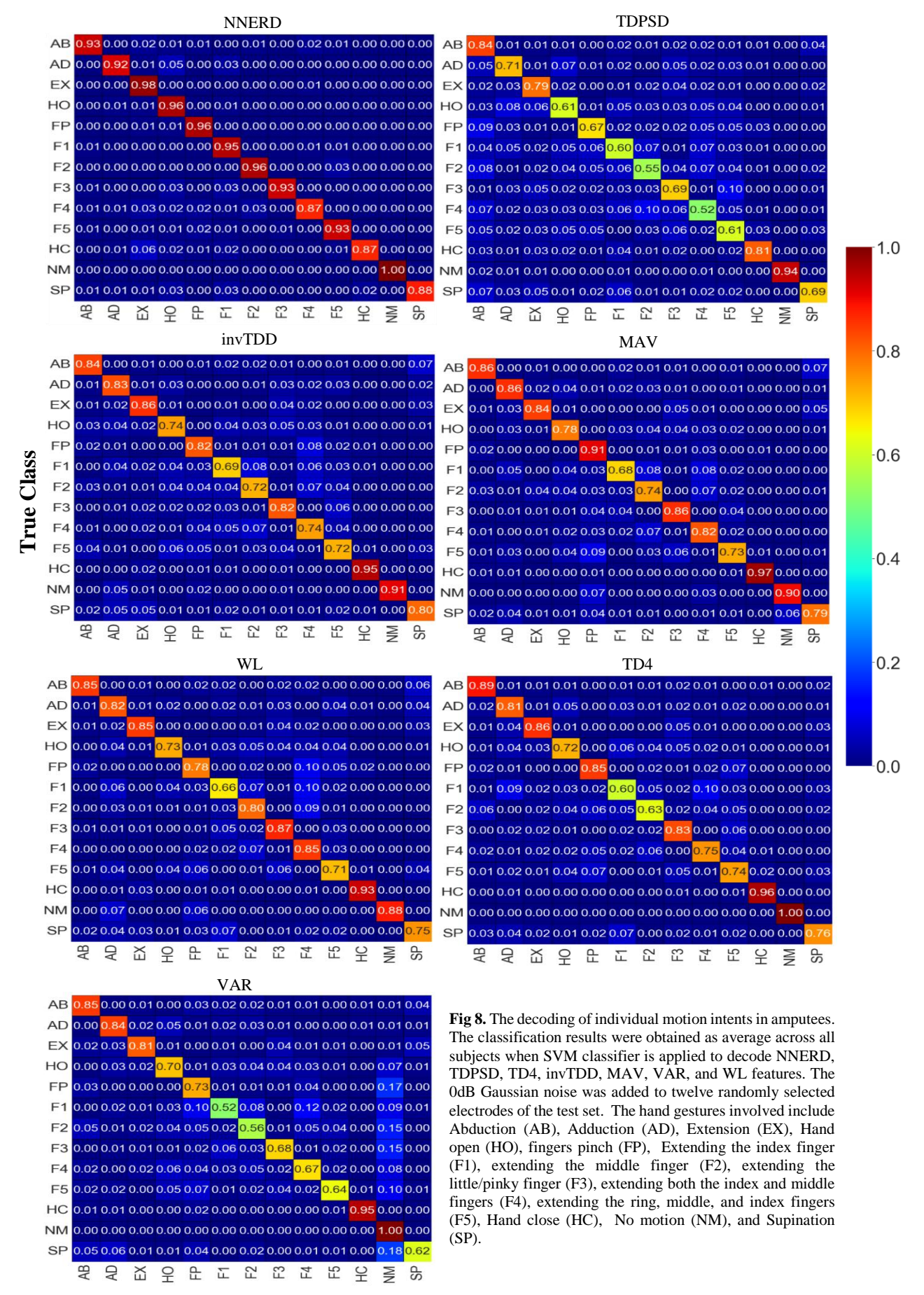
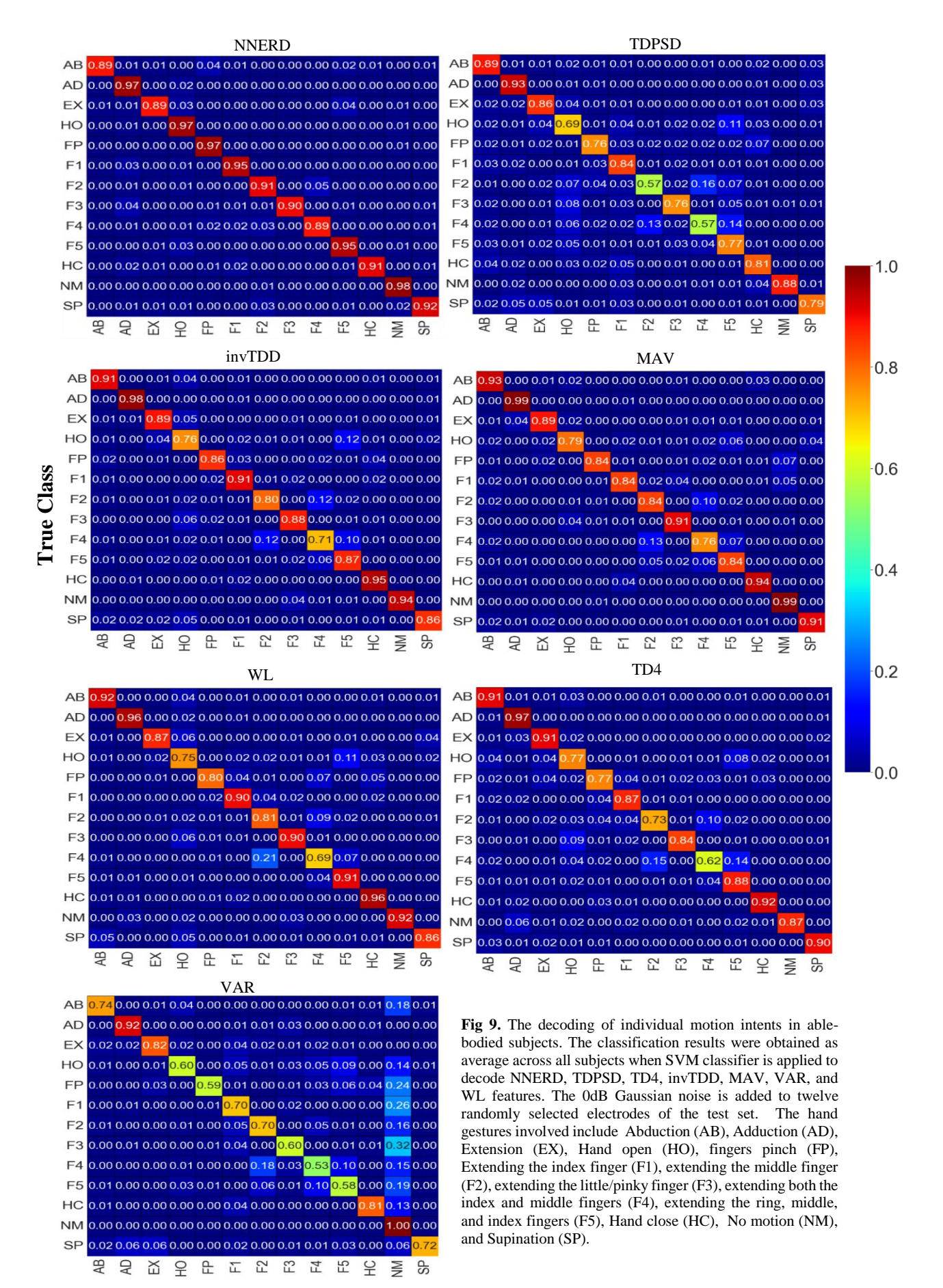


Fig 7. Classification accuracies of different features (NNERD, TDPSD, TD4, invTDD, MAV, VAR, and WL) applied on classifiers SVM, KNN and NMC when different number of electrodes of the test set are subjected to 20dB Gaussian noise. Note: The y-axis of all plots represent classification accuracies while the x-axis represent the quantity of electrodes with noise



**Predicted Class** 



**Predicted Class** 

When closely analyzing the classification outcomes in Fig. 7 (for 20dB SNR), the proposed feature extraction scheme (NNERD) has performed significantly better than other features (with p < 0.05). For instance, for the amputee's results, when one electrode was subjected to noise and SVM classifier was used, the decoding performances for the features (NNERD, TDPSD, TD4, invTDD, MAV, VAR, and WL) are 99.91±0.35%, 76.35±11.19%, 76.50±11.92%, 75.84±10.92%, 76.03±11.28%, 66.79±13.04%, 75.43±13.54% accuracy, while when twelve electrodes are subjected to noise, the decoding performances 99.52±0.86%, 75.69±11.32%, 76.47±11.69%, 75.67±11.13%, 76.19±11.21%, 67.28±13.26%, 75.95±12.50% accuracy, respectively.

## C. Analyzing the Performance of the features for individual motion decoding

In this section, we present the decoding performance of the NNERD and other features in decoding specific motion intent. Due to the consistently high performance of the NNERD in all classifiers and SNR levels, we considered the analysis using only SVM as a representative of other classifiers and 0dB (the worst level of noise) for representing SNR levels. The confusion matrices are indicated in Figs. 8 and 9 for amputees and able-bodied subjects, respectively.

From Fig. 8 for amputees, it can be seen that the NNERD has attained higher decoding performance in all thirteen classes of movements with the minimum class having an accuracy of 87.0%, while the minimum performing class for other features are 52.0%, 60.0%, 69.0%, 68.0%, 52.0%, and 66.0% for TDPSD, TD4, *inv*TDD, MAV, VAR, and WL, respectively. A similar pattern is observed in Fig. 9 for able-bodied subjects, where the proposed feature scheme has attained higher decoding performance in all individual classes, compared to the other features considered in this study.

**Generally,** NNERD has performed better (with a high margin) than other features. Its performance is similar in both amputees and able-bodied individuals, contrary to other features whose performances in able-bodied subjects are higher than in amputees. This indicates the potential and robustness of the proposed feature (NNERD).

Although the results are similar across all classifiers, a closer look at the decoding performance of the NMC classifier shows that NNERD has attained extremely high and stable performance compared to other features. Other features have extremely low results in the NMC classifier compared to other classifiers. The reason behind this might be that the dimension of the proposed feature is high and suitable for the NMC classifier, which was specifically designed to handle high-dimensional features [45], [37].

Additionally, when examining the variance of all features across all classifiers and SNR scenarios, the proposed feature NNERD has the lowest variance, justifying its consistent results across all subjects.

Apart from the feature and distribution adaptation (demonstrated in Section II-C) which reduces the discrepancy between the testing and training datasets, the outstanding performance of the proposed feature NNERD can also be attributed to the ability of SPDs to preserve not only temporal information from the EMG signals but also the correlation

between channels (spatial information) [46][47][48].

#### IV. ABLATION STUDY

This section analyzes the contribution of different stages of the proposed techniques to movement decoding performance. The ablation study was conducted on 15 amputees only. The results are presented as averages from these subjects. Additionally, in this section, we have included an analysis of the linear discriminant classifier (LDA) due to its comparatively good performance in hand gesture recognition.

# A. Evaluation of the impact of key stages of the proposed technique on the decoding performance

The feature adaptation scheme (*NNERD*) proposed in this study consists of three key operations/stages (Fig. 4). The first stage is the NMF operation, the second stage involves the construction of SPD and feature adaptation, and the third stage comprises the Distribution Adaptation operation/phase (DAP). To evaluate the contribution of each stage, we performed the ablation as follows.

First, we eliminated the NMF operation and the DAP in the pipeline. As such, the raw EMG of every segment (window) was converted to SPD matrices and passed through the feature adaptation operation. We termed this first approach FAP.

Secondly, we included the Distribution Adaption phase together with FAP and observed the contribution of DAP on FAP. We denote this approach as DAP.

Lastly, to improve the performance, the NMF operation was incorporated as a preprocessing technique comprising the whole proposed feature (NNERD). The results for each stage are displayed in Table 4 for the classifiers SVM, kNN, NMC, and LDA.

**Table 4.** The ablation study on the three stages of the proposed method (in accuracy %)

	FAP	DAP	NNERD
SVM	91.99±7.50	94.25±7.78	99.91±0.35
kNN	87.17±8.76	90.21±9.95	99.79±0.46
NMC	71.66±16.76	88.23±11.20	99.32±0.96
LDA	90.41±8.79	94.19±8.57	98.34±5.24

Looking closely at the results in Table 4, it can be observed that there is a substantial increase in decoding performance when applying the distribution adaptation (DAP) from the feature adaptation (FAP). An additional increase is observed when NMF is applied to complete the whole process of NNERD. For instance, when considering the SVM, we can observe the increase from 91.99±7.50%, 94.25±7.78%, to 99.91±0.35% when applying FAP, DAP and NMF (to constitute NNERD), respectively.

Similar increments are observed in other classifiers. Therefore, every stage has a significant contribution.

## B. Evaluation of the Impact of NMF on the Decoding Performance of Other State-of-the-Art Techniques

This section evaluates the impact of applying NMF during the preprocessing stage on the performance of other state-ofthe-art techniques. Table 5 presents the decoding accuracy results for these methods while considering two scenarios, with the application of NMF and without the application of NMF. NMC

LDA

Table 5. The decoding accuracy (%) for other state-of-the-art methods. (a) Without NMF applied (b) With NMF applied

48.05±17.89

82.34+1.75

	ible ev The decoding t	(70) Tot other	state of the art method	(a) Whiteat I will app	nea (e) what will ap	Jirea	
		(a)	) Without_NMF				
	TDPSD	TD4	invTDD	MAV	VAR	WL	
SVM	76.40±11.12	76.43±11.96	75.82±10.94	76.02±11.25	66.78±13.04	75.43±13.46	
KNN	67.01±13.87	68.88±14.10	59.44±13.77	68.32±13.93	60.29±13.92	70.29±13.29	
NMC	55.30±13.71	49.44±13.32	45.95±11.82	46.89±12.16	42.37±10.69	43.87±12.01	
LDA	80.05±9.97	80.73±9.49	81.82±9.26	78.36±10.15	67.19±12.87	78.28±11.05	
(b) With_NMF							
	TDPSD	TD4	invTDD	MAV	VAR	WL	
SVM	77.13±2.66	76.75±3.49	73.84±3.35	78.01±3.77	67.63±6.04	77.35±2.93	
KNN	64.99±6.67	72.01±4.86	61.22±9.68	69.19±5.00	62.82±7.36	68.83±5.42	

47.10±18.67

75.27+2.97

By carefully analyzing the results in Table 5, it can be seen that the application of NMF improves the performance of the features. However, the margin of improvement is not significant (the majority are between 0.09% to 2.00%), while some features show a decrement in certain classifiers.

 $53.39 \pm 17.65$ 

81.07+2.52

 $57.17 \pm 15.38$ 

80.28+1.91

Due to the inconsistent non-significant increase when applying NMF on other state-of-the-art features, we did not include NMF as part of the extraction of other state-of-the-art features in the previous sections.

It is worth noting that we acknowledge the use of LDA in decoding the movement, as applied by previous works. However, due to the comparatively similar performance of LDA, KNN, and SVM, we decided to limit our analysis to only three classifiers (SVM, KNN, and NMC).

## C. Computational Time

This section investigates the computational time for different techniques. Two phases are considered. The first phase is the time taken for preprocessing, feature extraction, and training the classifier. It involves the training dataset only and is denoted as Train-Time. The second phase is the time taken for preprocessing, feature extraction, and testing (prediction), which involves the testing dataset only. This time is denoted as Test-Time. Table 6 indicates the two phases. Additionally, we have included the analysis of the proposed feature but excluded the NMF operation from it, and we denote this as Non-Euclidean Riemannian Feature (NERF).

**Table 6.** Computational time (seconds) for training and test phases

Time	NERF	NNERD	TDPSD	TD4	invTDD	MAV	VAR	WL
Train	33.83	53.12	4.23	40.32	17.67	2.36	3.50	2.59
Test	2.70	21.46	2.45	11.00	5.45	1.56	1.86	1.65

From the results in Table 6, the proposed feature NNERD has the highest computational time. The reason behind this may be due to the addition of the NMF operation. As we can observe, if the NMF is excluded from the proposed feature (to constitute a NERF), its testing computational time becomes comparatively lower than other features such as TD4 and *inv*TDD.

#### V. CONCLUSION

This study introduces a feature extraction approach to improve the effectiveness of the EMG-based motion intent classification system. The proposed approach utilizes nonnegative matrix factorization (NMF) and symmetric positive definite (SPD) matrices, which exist in a non-Euclidean space, enabling the extraction of features for motion intents from

electromyogram signals. To reduce the drift/discrepancy between the testing and training datasets, NMF is first applied to the EMG signal, followed by feature adaptation that relies on the Riemann mean of the training set. To further reduce the discrepancy, the final stage projects all the features of the training and testing sets towards a common distribution whose parameters are derived from the training set only.

42.46±15.46

70.06+6.25

47.33±18.47

79.19+2.23

The proposed feature scheme has been validated using a dataset that was collected from both amputees and able-bodied subjects, and it has demonstrated outstanding performance compared to other features when there is no noise (in amputees), with maximum accuracies of 99.91±0.35% for SVM, 99.79±0.46% for kNN, and 99.32±0.96% for the NMC classifier. In able-bodied subjects, the results are 99.99±0.02% for SVM, 99.91±0.18% for kNN, and 99.51±0.69% for the NMC classifier. When subjected to noise, the proposed feature (NNERD) still showed higher decoding results than other features, with the lowest performance of 93.87±4.30% accuracy (for able-bodied subjects) and 92.32±5.43% accuracy (for amputees) at a severe noise level (SNR of 0dB). This performance is still higher than all other features at their highest performing state (20dB of SNR). These results justify the effectiveness of the NNERD, which could enhance motor intent decoding performance in the EMG-based system.

While the NNERD technique has demonstrated promising classification performance, it was tested on offline experimental setups. Therefore, our future research will focus on validating the effectiveness of the proposed method in real-time clinical/practical settings.

#### REFERENCES

- [1] A.H. Al-Timemy et al., "Improving the performance against force variation of EMG controlled multifunctional upper-limb prostheses for transradial amputees." IEEE Transactions on Neural Systems and Rehabilitation Engineering 24.6 (2015): 650-661.
- [2] E. Scheme and K, Englehart, "Electromyogram pattern recognition for control of powered upper-limb prostheses: state of the art and challenges for clinical use." Journal of Rehabilitation Research & Development 48.6 (2011).
- [3] O. W. Samuel et al., "Pattern recognition of electromyography signals based on novel time domain features for amputees' limb motion classification." Computers & Electrical Engineering 67 (2018): 646-655.
- [4] X. Li et al., "A motion-classification strategy based on sEMG-EEG signal combination for upper-limb amputees." Journal of neuroengineering and rehabilitation 14.1 (2017): 1-13.
- [5] M.G. Asogbon et al., "Towards resolving the co-existing impacts of multiple dynamic factors on the performance of EMG-pattern recognition based prostheses." Computer methods and programs in biomedicine 184 (2020): 105278.
- [6] J. He et al., "Invariant surface EMG feature against varying contraction level for myoelectric control based on muscle coordination." IEEE journal of biomedical and health informatics 19.3 (2014): 874-882.
- [7] R. N. Khushaba et al., "Combined influence of forearm orientation and muscular contraction on EMG pattern recognition." Expert Systems with Applications 61 (2016): 154-161.
- [8] K. Englehart and B. Hudgins, "A robust, real-time control scheme for multifunction myoelectric control." IEEE transactions on biomedical engineering 50.7 (2003): 848-854.

- [9] O. W. Samuel et al., "Spatio-temporal based descriptor for limb movement-intent characterization in EMG-pattern recognition system." 2019 41st Annual International Conference of the IEEE Engineering in Medicine and Biology Society (EMBC). IEEE, 2019
- [10] P. Trujillo et al., "Quantitative EEG for predicting upper limb motor recovery in chronic stroke robot-assisted rehabilitation." IEEE transactions on neural systems and rehabilitation engineering 25.7 (2017): 1058-1067.
- [11] S. Kumar, Y. Florian and L. Fabien, "Towards adaptive classification using Riemannian geometry approaches in brain-computer interfaces." In 2019 7th International Winter Conference on Brain-Computer Interface (BCI), pp. 1-6. IEEE, 2019.
- [12] H. Ramoser, J. Muller-Gerking and G. Pfurtscheller, "Optimal spatial filtering of single trial EEG during imagined hand movement." IEEE transactions on rehabilitation engineering 8, no. 4 (2000): 441-446.
- [13] Y. Florian, L. Fabien and S. Masashi, "Averaging covariance matrices for EEG signal classification based on the CSP: an empirical study." In 2015 23rd European Signal Processing Conference (EUSIPCO), pp. 2721-2725. IEEE, 2015
- [14] Z. Huang et al., "Log-euclidean metric learning on symmetric positive definite manifold with application to image set classification." In International conference on machine learning, pp. 720-729. PMLR, 2015.
- [15] J. Li, R. Wang and L. Pan, "An enhanced EMG-driven musculoskeletal model based on non-negative matrix factorization." Biomedical Signal Processing and Control 79 (2023): 104178.
- [16] F. Kulwa et al., "A Multidataset Characterization of Window-Based Hyperparameters for Deep CNN-Driven sEMG Pattern Recognition." IEEE Transactions on Human-Machine Systems (2023).
- [17] G. Huang et al., "Low-density surface electromyographic patterns under electrode shift: Characterization and NMF-based classification." Biomedical Signal Processing and Control 59 (2020): 101890.
- [18] M. S. Singh, R. Pasumarthy and V. Talasila. "Time series analysis of surface EMG signal-linear, non linear and chaotic approaches." In 2019 Fifth Indian Control Conference (ICC), pp. 442-447. IEEE, 2019.
- [20] X. Li et al., "Towards reducing the impacts of unwanted movements on identification of motion intentions." Journal of Electromyography and Kinesiology 28 (2016): 90-98.
- [21] A. Ameri et al., "A deep transfer learning approach to reducing the effect of electrode shift in EMG pattern recognition-based control." IEEE Transactions on Neural Systems and Rehabilitation Engineering 28, no. 2 (2019): 370-379.
- and Rehabilitation Engineering 28, no. 2 (2019): 370-379. [22] A. Barachant et al., "Riemannian geometry applied to BCI classification." International conference on latent variable analysis and signal separation. Berlin, Heidelberg: Springer Berlin Heidelberg, 2010
- [23] H. Cha, and C. Im, "Improvement of robustness against electrode shift for facial electromyogram-based facial expression recognition using domain adaptation in VR-based metaverse applications." Virtual Reality (2023): 1-12.
- [24] P. Zanini et al., "Transfer learning: A Riemannian geometry framework with applications to brain-computer interfaces." IEEE Transactions on Biomedical Engineering 65, no. 5 (2017): 1107-1116.
- [25] M. Moakher, "A differential geometric approach to the geometric mean of symmetric positive-definite matrices." SIAM journal on matrix analysis and applications 26, no. 3 (2005): 735-747.
- [26] R. Wang et al., "Covariance discriminative learning: A natural and efficient approach to image set classification." In 2012 IEEE conference on computer vision and pattern recognition, pp. 2496-2503. IEEE, 2012.
- [27] R. Tibshirani et al., "Diagnosis of multiple cancer types by shrunken centroids of gene expression." Proceedings of the National Academy of Sciences 99, no. 10 (2002): 6567-
- [28] O. W. Samuel et al., "Multiresolution Dual-Polynomial Decomposition Approach for Optimized Characterization of Motor Intent in Myoelectric Control Systems." IEEE Transactions on Biomedical Engineering 70, no. 5 (2022): 1516-1527.
- [29] B. Hudgins, P. Parker, and R. N. Scott. "A new strategy for multifunction myoelectric control." IEEE transactions on biomedical engineering 40, no. 1 (1993): 82-94.
- [30] R. Khushaba et al., "Towards limb position invariant myoelectric pattern recognition using time-dependent spectral features." *Neural networks* 55 (2014): 42-58.
- [31] M. G. Asogbon et al., "Towards resolving the co-existing impacts of multiple dynamic factors on the performance of EMG-pattern recognition based prostheses." Computer methods and programs in biomedicine 184 (2020): 105278.
- [32] M. Zardoshti-Kermani et al., "EMG feature evaluation for movement control of upper extremity prostheses." IEEE Transactions on Rehabilitation Engineering 3, no. 4 (1995): 324-333.
- [33] M. G. Asogbon et al., "Appropriate feature set and window parameters selection for efficient motion intent characterizatin towards intelligently smart EMG-PR system." Symmetry 12, no. 10 (2020): 1710.
- [34] R. Khushaba et al., "Combined influence of forearm orientation and muscular contraction on EMG pattern recognition." Expert Systems with Applications 61 (2016): 154-161.
- [35] C. Ma et al., "A novel and efficient feature extraction method for deeplearning based continuous estimation." IEEE Robotics and Automation Letters 6, no. 4 (2021): 7341-7348.
- [36] A. Phinyomark et al., "Feature extraction of the first difference of EMG time series for EMG pattern recognition." Computer methods and programs in biomedicine 117, no. 2 (2014): 247-256.
- [37] V. Praveen, K. Kousalya and K. R. Prasanna Kumar, "A nearest centroid classifier based clustering algorithm for solving vehicle routing problem." In 2016 2nd International Conference on Advances in Electrical, Electronics, Information, Communication and Bio-Informatics (AEEICB), pp. 414-419. IEEE, 2016.
- [38] S. Tan, Y. Wang, and G. Wu. "Adapting centroid classifier for document categorization." Expert Systems with Applications 38, no. 8 (2011): 10264-10273.

- [39] Z. Zhao, W. Guo, Y. Xu, and X. Sheng. "A biosignal quality assessment framework for high-density sEMG decomposition." Biomedical Signal Processing and Control 90 (2024): 105800.
- [40] N. Zhang et al., "A novel antibacterial membrane electrode based on bacterial cellulose/polyaniline/AgNO 3 composite for bio-potential signal monitoring." IEEE Journal of Translational Engineering in Health and Medicine 6 (2018): 1-10.
- [41] Y. Jiang et al., "Effective biopotential signal acquisition: comparison of different shielded drive technologies." Applied Sciences 8, no. 2 (2018): 276.
- [42] Y. Fu et al., "Dry electrodes for human bioelectrical signal monitoring." Sensors 20, no. 13 (2020): 3651.
- [43] G. J. Jin., M. J. Uddin, and J. S. Shim. "Biomimetic cilia-patterned rubber electrode using ultra conductive polydimethylsiloxane." Advanced Functional Materials 28, no. 50 (2018): 1804351.
- [44] L. Yang et al., "Insight into the contact impedance between the electrode and the skin surface for electrophysical recordings." ACS omega 7, no. 16 (2022): 13906-13912.
- [45] S. Ren and Q. Mai. "The robust nearest shrunken centroids classifier for high-dimensional heavy-tailed data." Electronic Journal of Statistics 16, no. 1 (2022): 3343-3384
- [46] Y. Gao et al., "EEG emotion recognition based on enhanced SPD matrix and manifold dimensionality reduction." Computers in biology and medicine 146 (2022): 105606.
- [47] T. Zhang et al., "Deep manifold-to-manifold transforming network for skeleton-based action recognition." IEEE Transactions on Multimedia 22, no. 11 (2020): 2926-2937.
- [48] S. Cheng et al., "Action recognition based on spatio-temporal log-Euclidean covariance matrix." International Journal of Signal Processing, Image Processing and Pattern Recognition 9, no. 2 (2016): 95-106.
- [49] F. Kulwa et al., "A robust feature adaptation approach against variation of muscle contraction forces for myoelectric pattern recognition-based gesture characterization." Biomedical Signal Processing and Control 95 (2024): 106446.0.5
- [50] C. Simar et al., "Hyperscanning EEG and classification based on Riemannian geometry for festive and violent mental state discrimination." Frontiers in Neuroscience 14 (2020): 588357.
- [51] Z, Al-Mashhadani et al., "The Efficacy and Utility of Lower-Dimensional Riemannian Geometry for EEG-Based Emotion Classification." Applied Sciences 13, no. 14 (2023): 8274.
- [52] H. J. Kim et al., "Riemannian nonlinear mixed effects models: Analyzing longitudinal deformations in neuroimaging." In Proceedings of the IEEE conference on computer vision and pattern recognition, pp. 2540-2549. 2017.